Oxygenases

DpgC-Catalyzed Peroxidation of 3,5-Dihydroxyphenylacetyl-CoA (DPA-CoA): Insights into the Spin-Forbidden Transition and Charge Transfer Mechanisms**

Pablo Ortega,[a] Alexandre Zanchet,[a, b] Cristina Sanz-Sanz,[c] Susana Gómez-Carrasco,[a] Lola González-Sánchez,[a] and Pablo G. Jambrina*[a]

Abstract: Despite being a very strong oxidizing agent, most organic molecules are not oxidized in the presence of O_2 at room temperature because O_2 is a diradical whereas most organic molecules are closed-shell. Oxidation then requires a change in the spin state of the system, which is forbidden according to non-relativistic quantum theory. To overcome this limitation, oxygenases usually rely on metal or redox cofactors to catalyze the incorporation of, at least, one oxygen atom into an organic substrate. However, some oxygenases do not require any cofactor, and the detailed mechanism followed by these enzymes remains elusive. To fill this gap, here the mechanism for the enzymatic cofactor-independent oxidation of 3,5-dihydroxyphenylacetyl-CoA (DPA-CoA) is studied by combining multireference calculations on a model system with QM/MM calculations. Our results reveal that intersystem crossing takes place without requiring the previous protonation of molecular oxygen. The characterization of the electronic states reveals that electron transfer is concomitant with the triplet–singlet transition. The enzyme plays a passive role in promoting the intersystem crossing, although spontaneous reorganization of the water wire connecting the active site with the bulk presets the substrate for subsequent chemical transformations. The results show that the stabilization of the singlet radical-pair between dioxygen and enolate is enough to promote spin-forbidden reaction without the need for neither metal cofactors nor basic residues in the active site.

1. Introduction

The great oxygenation event, approximately 2.4 billion years ago, was one of the most important episodes in the history of life on Earth.[1] The accumulation of molecular oxygen (O_2) in the atmosphere eventually caused the extinction of a myriad of life forms.[2] Those that survived evolved to exploit the presence of O_2, using it to release the energy that cells will use for their maintenance and growth. The oxygen reduction reaction is also crucial for emerging energy technologies, such as solar fuels production.[3–5]

From a chemical point of view, reactions between O_2 and organic matter are conceptually complicated. The majority of the stable molecules involved in a biological process are singlets (all the electrons are paired). O_2 is an exception to this rule, and in its ground electronic state it has two unpaired electrons: it is a triplet. Hence, reactions between O_2 and organic molecules should involve the change of the spin state (intersystem crossing), a process that is forbidden in non-relativistic quantum chemistry, and accordingly should be very slow at room temperature. This explains why organic matter exists in our oxidizing atmosphere.

To circumvent this limitation, enzymes typically use transition metals, mostly iron, to catalyze reactions with O_2.[6–15] Transition metals also contain unpaired electrons so may react with O_2 via a spin-allowed reaction. Moreover, metals can be used to preactivate the substrate, forming a radical that can react with O_2.[6,14,16] Last but not least, spin-orbit coupling (SOC),[17,18] the relativist effect that permits intersystem crossing, is expected to be significantly strong for systems that include transition metals. Other proteins use redox organic cofactors to catalyze spin-forbidden reactions, especially flavin.[19–21]

Intriguingly, some oxygenases are capable of catalyzing the incorporation of at least one oxygen atom from O_2 to an organic substrate without needing any cofactor.[22–24] The catalyt-

[a] P. Ortega, Dr. A. Zanchet, Dr. S. Gómez-Carrasco, Dr. L. González-Sánchez, Dr. P. G. Jambrina
Departamento de Química Física
University of Salamanca
Salamanca 37008 (Spain)
E-mail: pjambrina@usal.es

[b] Dr. A. Zanchet
Instituto de Física Fundamental (CSIC)
Madrid, 28006 (Spain)

[c] Dr. C. Sanz-Sanz
Departamento de Química Física Aplicada
University Autónoma de Madrid
Madrid 28049 (Spain)

[**] A previous version of this manuscript has been deposited on a preprint server (https://doi.org/10.1002/chem.202002993).

Supporting information and the ORCID identification number(s) for the author(s) of this article can be found under: https://doi.org/10.1002/chem.202002993.

ic mechanism followed by these enzymes has been studied both computational and experimentally (see for example Refs. [25]–[38]) although the procedure used to facilitate intersystem crossing is still controversial.[29,35]

From among these proteins, we will focus on DpgC, the first protein for which a crystal structure showing a substrate analog and O_2 bound to the enzyme was resolved.[36–38] DpgC is a hexameric crotonase oxygenase[39,40] that plays a key role in the biosynthesis of dihydroxyphenylglycine (DPG), a non-natural amino acid found in "antibiotics of last resort" such as vancomycin or teicoplanin.[41] In particular, DpgC catalyzes the cofactor-independent oxidation of 3,5-dihydroxyphenylacetyl-CoA (DPA-CoA) to 3,5-dihydroxyphenyl-glyoxylate (DPGX; Figure 1). When DPA-CoA binds to the active site, it is deprotonated at C_α. Deuterium atom exchange was observed even at anaerobic conditions, confirming that this first step is O_2 independent and that DpgC stabilizes the enolate before O_2 accesses the active site.[42] Following deprotonation of C_α, O_2 diffuses into the active site. Molecular dynamics (MD) calculations predict that there are three main pathways for O_2 diffusion,[43] all of them guiding O_2 to the hydrophobic pocket in which O_2 was resolved in the crystal structure. These simulations also suggested that the binding of O_2 to the active site is rather weak, which is compensated by a higher frequency of O_2 entry into the active site.[43]

The reaction between O_2 and DPA-CoA is expected to proceed via a peroxide intermediate.[36,38] This is a spin-forbidden process, and it is likely the rate-limiting stage of the overall process. Contrary to what was observed for other proteins such as glucose oxidase[33] where a His516 residue acts as a proton donor and protonates O_2 throughout the reaction, in the O_2 pocket of DpgC there are no amino acids that could play that role. In a subsequent step, the peroxide breaks leading to the formation of DPGX via either a Criegee rearrangement or following a dioxetane intermediate.[42]

There are three reasons why we believe that DpgC is an excellent system for the characterization of the general mechanism of a spin-forbidden cofactorless addition of O_2 to an organic enolate. First, the lack of basic residues around the active site permits us to analyze to what extent the formation of the peroxide is possible in the absence of amino acids, which could protonate the peroxide. Second, there are no aromatic residues that could be involved in π–π stacking interactions, so the hypothesis of a "spin-well" could be ruled out.[25] Third, the peroxidation occurs outside the aromatic ring, so in a first approximation the π orbitals of the ring do not have to be included in the active space, which facilitates convergence in the multireference calculations.

From a fundamental point of view, the study of spin-forbidden reactions is very challenging. It requires the characterization of all the concurrent potential energy surfaces (PESs), for at least two different spin multiplicities. For these reactions, the minimum energy crossing point (MECP) between the two PESs of different spin multiplicities plays the role of the effective barrier.[44–49] To determine the rate coefficient of a spin-forbidden reaction, it is also necessary to calculate the SOC. In the non-adiabatic transition state theory, the transmission coefficient is approximated by the hopping probability, which depends on the magnitude of the SOC, and also on the difference in slope of the PESs along with the reaction coordinate in the crossing point. In its simplest case, the hopping probability is calculated by using the celebrated Landau–Zener formula.[50] For typical values of SOC, the hopping probability lies between 0.001 and 0.1, which is equivalent to an increase in the activation energy of 1–4 kcal mol^{-1} at room temperature.[47,49] Similar methodologies have been successfully applied to the study of some enzymatic reactions,[15,28–33,44,52,53] including glucose oxidase[32,33] and *p*-hydroxyphenylacetate hydroxylase,[28] for which O_2 reacts with flavin, as well as the cofactorless oxygenases (1*H*)-3-hydroxy-4-oxoquinaldine 2,4-dioxygenase (HOD)[29,31] and nogalamycin monoxygenase,[30] some of them using small active site models.

Regarding the available ab initio methods that could be used to describe spin-forbidden reactions, multireference methods are advised as they account for several electronic states on an equal footing, and estimate the magnitude of the SOC. Among these methods, the multiconfiguration reference internally contracted configuration interaction (MRCI) method is one of the most accurate, and it is considered the golden standard for multireference systems. MRCI is routinely applied for the calculation of ground and excited PESs for systems involving up to three or four atoms in several electronic states (see for example Refs. [54]–[59]). For larger systems, the use of MRCI is not common owing to its computational cost, and convergence issues. However, if it is possible to select a stable active space that properly describes the process under study, it becomes a powerful tool for the understanding of chemical reactivity.

The goal of this article is to understand the detailed mechanism of the spin-forbidden reactions between O_2 and an organic substrate that does not require the presence of any cofactor. To address this question, we studied the reaction between DPA-CoA and O_2 by using two sets of quantum calculations: high level multireference ab initio methods on a model system, and a DFT-based QM/MM approach.

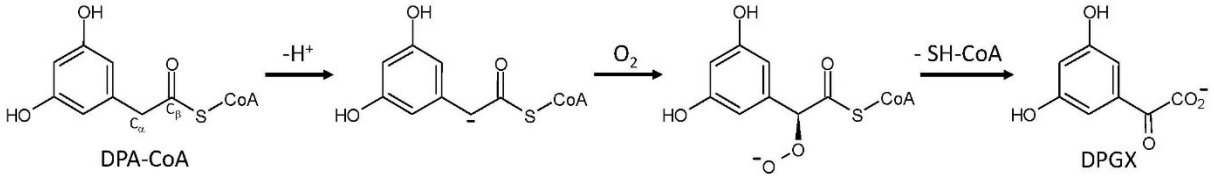

Figure 1. Proposed mechanisms for the conversion of 3,5-dihydroxyphenylacetyl-CoA (DPA-CoA) to 3,5-dihydroxyphenyl-glyoxylate (DPGX) by DpgC.

2. Results and Discussion

As stated above, we are going to combine the results obtained by using two kinds of calculations. The first group consisted of MRCI calculations describing the nine electronic states that are relevant for O_2 addition to the enolate. Owing to the large computational cost of MRCI calculations, we used the model system depicted in the top panel of Figure 2, where DPA-CoA has been replaced by *S*-methyl-but-3-enethioate (hereinafter butenthioate). The second group of calculations consisted of a QM/MM description of the enzymatic reaction, relying on DFT methods. The atoms included in the QM region (shown in the bottom panel of Figure 2) are O_2, the DPA moiety of the substrate, and the sidechain of three residues: Ala319 and Ile324 in the hydrophobic pocket of O_2, and Gln299. We also added to the QM region four water molecules nearby, which could be involved either in the protonation of the peroxide formed or in the stabilization of DPA-CoA. The QM/MM calculations will provide clues to the role played by the protein scaffold to promote the process, and in particular, will serve to discuss the relevance of the possible proton transfer steps.

2.1. Reaction between O_2 and *S*-methyl-but-3-enethioate

In its ground state, the electronic configuration of O_2 is $(1\sigma_g)^2(1\sigma_u^*)^2(2\sigma_g)^2(2\sigma_u^*)^2(3\sigma_g)^2(1\pi_u)^4(1\pi_g^*)^2$. The distribution of two electrons in two degenerated π orbitals leads to three electronic states relatively close in energy: the ground $^3\Sigma_g^-$ state, the $^1\Delta_g$ (doubly degenerate, which splits into two states in the presence of any colliding partner), and the $^1\Sigma_g^+$. The energy difference between $^1\Sigma_g^+$ and $^3\Sigma_g^-$ is only of 37.7 kcal mol^{-1},[60] with $^1\Delta_g$ lying between them (22.64 kcal mol^{-1} above $^3\Sigma_g^-$). Further excited states involve excitation of one electron from the $(1\pi_g^*)$ to $(3\sigma_u^*)$ orbital, but they appear much higher in energy and are unlikely to play any role in the intersystem crossing. On the other hand, butenthioate is a closed-shell molecule that does not present any excited state close in energy.

For the MRCI calculations, we selected an active space that includes four electrons in three orbitals: the HOMO orbital of butenthioate (hereinafter $p_{C\alpha}$, although it is delocalized over the three sp^2 C atoms) and the two $1\pi_g^*$ orbitals of O_2, which are singly occupied in the ground state of O_2 and we will denote as $\pi_{O_2}^*$. With this active space we can describe up to nine electronic states: three triplets and six singlet states, denoted as 1–3^3[DPA-O_2] and 1–6^1[DPA-O_2], respectively.

Figure 3 displays the energy profiles of the considered electronic states during the addition of O_2 to butenthioate as a function of $r_{C_\alpha O}$, the distance between C_α and O_2 (the two atoms between which the new bond will be formed, as shown in Figure 2). To build these energy profiles, optimized geometries were considered for each value of $r_{C_\alpha O}$, following the procedure described in the Experimental Section. It is worth noticing that, based on QM/MM optimizations of the peroxide, we applied constraints to keep all the C atoms of butenthioate in the same plane. This constraint is only relevant at small $r_{C_\alpha O}$, where the peroxide is formed, and was chosen to better mimic the behavior of DPA-CoA in the protein environment (see the Experimental Section).

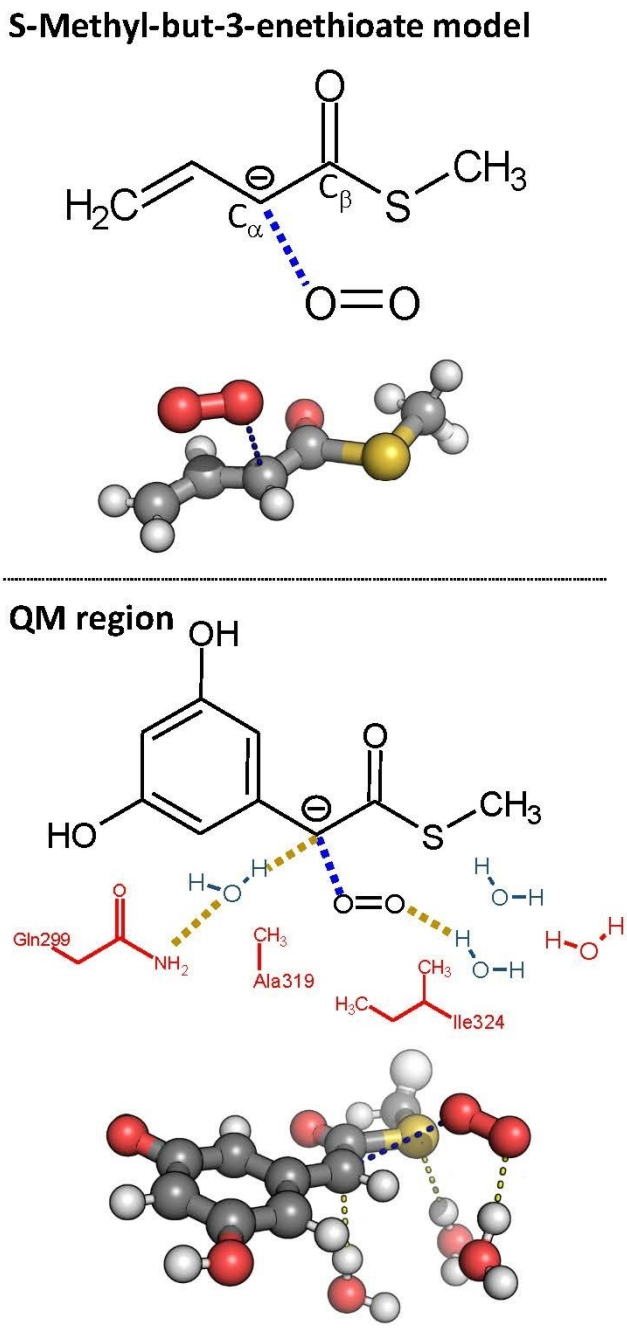

Figure 2. Schematic representation of the atoms included in the *S*-methyl-but-3-enethioate (top panel), and in the QM region for the QM/MM calculations (bottom panel). Two different QM regions were used in the later calculations. A larger one including all residues highlighted, and a smaller one in which the residues highlighted in red were included in the MM region. The hydrogen bonds between DPA and the water molecules nearby are highlighted in yellow, whereas the distance between C_α and O_2 is highlighted in blue. For the sake of clarity, we only show in the 3D representation the atoms included in the small QM region.

At large $r_{C_\alpha O}$ distances, it is safe to assume that there is almost no interaction between butenthioate and O_2, and the active orbitals do not mix. Under these circumstances, it is pos-

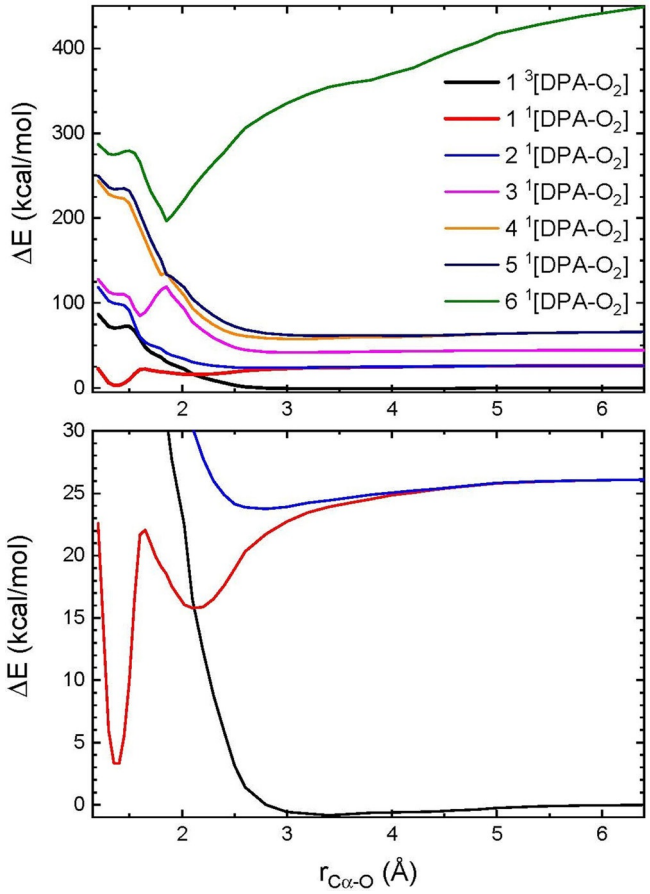

Figure 3. Top panel: Energy profiles for the addition of O_2 to *S*-methyl-but-3-enethioate as a function of the C_α–O distance. The ground triplet state and the six singlets involved are shown. A zoom of the lower energy region is shown in the bottom panel. The two excited triplet states are not depicted for the sake of clarity. Calculations carried out at the MRCI(4,3)/6-31+G(d,p) level of theory.

sible to correlate the adiabatic states with the electronic configurations of the two colliding partners. The first four states (the ground triplet state, 1^3[DPA-O_2], and the three first singlet states, 1–3^1[DPA-O_2]) are well described with a $(p_{C\alpha})^2(\pi_{O_2}{}^*)^2$ electronic configuration, namely DPA^--O_2, where the negative charge is located on the butenthioate. In this conformation, the four states correlate to the four lowest energy states of O_2: the ground $^3\Sigma_g^-$ state, the $^1\Delta_g$ (doubly degenerate), and the $^1\Sigma_g^+$. In our calculations, the energy difference between $^1\Delta_g$ and $^3\Sigma_g^-$ is 26.1 kcal mol^{-1}, just a 15% larger than that observed for gas-phase isolated O_2,[60] and the same trend is observed for the difference between $^1\Sigma_g^+$ and $^3\Sigma_g^-$, which confirms the validity of the applied theoretical methods.

The following four states, 4–5^1[DPA-O_2] and 2–3^3[DPA-O_2] can be described by using a $(p_{C\alpha})^1(\pi_{O_2}{}^*)^3$ electronic configuration, namely DPA-O_2^-, which corresponds to a radical-pair between the superoxide anion O_2^- and the butenthionyl radical. As there is no interaction between butenthioate and O_2, all of them are degenerate at large $r_{C_\alpha O}$. The energy difference between 1^3[DPA-O_2] and these states is 66.1 kcal mol^{-1}, and corresponds to the energy required to transfer one electron from butenthioate to O_2 in the gas phase. The presence of the protein environment stabilizes the charge on the O_2^-, shifting this energy to 36.6 kcal mol^{-1}. This value, however, is significantly larger than that calculated for the reaction between O_2 and flavin, 2.8 kcal mol^{-1} at a DFT level (and implicit water solvent).[30] This difference may explain why enzymes use flavin as a redox catalyzer.

The electronic configuration of the last state, 6^1[DPA-O_2], is $(p_{C\alpha})^0(\pi_{O_2}{}^*)^4$ or DPA^+-O_2^{2-}. It corresponds to the interaction between the peroxide anion (O_2^{2-}) and the butenthionyl cation. The energy of this state is very high (more than 450 kcal mol^{-1}), as it requires the transference of two electrons from butenthioate to O_2. Its energy, however, decreases quickly with $r_{C_\alpha O}$ distance, as expected for an ion–ion interaction ($E \propto r^{-1}$). If we had used a larger active space, we would have obtained several states between 5^1[DPA-O_2] and 6^1[DPA-O_2], and this would have impaired the description of the 6^1[DPA-O_2]. Despite the very large energy difference between 6^1[DPA-O_2] and the ground 1^3[DPA-O_2] state, the former state will be important to describe the formation of the peroxide, as we will discuss below.

When O_2 and butenthioate approach each other, the orbitals mix and the correspondence between our adiabatic states and the electronic configuration of the two independent molecules is no longer valid. This motion is associated with a change in the relative orientation of O_2 with respect to butenthioate (see Figure S1 in the Supporting Information). At $r_{C_\alpha O} < 4$ Å, the interaction between O_2 and butenthioate is already strong enough to break the degeneracy of 2–3^1[DPA-O_2] (former $^1\Delta_g$ states). The inspection of the active space orbitals reveals that $p_{C\alpha}$ starts to overlap with one of the two no longer equivalent $\pi_{O_2}{}^*$. The same effect is observed for the four DPA-O_2^- states, also no longer degenerate. The interaction of butenthioate and O_2 means that for 2 Å $< r_{C_\alpha O} <$ 3 Å only 1^1[DPA-O_2] and 6^1[DPA-O_2] are not repulsive. For $r_{C_\alpha O} < 2$ Å, the ground singlet state becomes more stable than the triplet state, showing a minimum for $r_{C_\alpha O} = 1.4$ Å. 6^1[DPA-O_2] reaches a minimum at 1.85 Å, after which its energy rises. This behavior is not compatible with the description of an ion–ion interaction, suggesting that this state has changed its character owing to an avoided crossing caused by strong non-adiabatic couplings with other singlet states.

The bottom panel of Figure 3 shows an expanded view that allows us to appreciate the main features of the PESs for the three lowest energy states, 1^3[DPA-O_2] and 1–2^1[DPA-O_2]. The 1^3[DPA-O_2] state is purely repulsive, and its energy rises quickly at $r_{C_\alpha O} < 2.5$ Å. That behavior is shared with the 2^1[DPA-O_2] state. On the contrary, 1^1[DPA-O_2] is attractive and displays a double-well structure. The energy of the minimum of the first well is 15.9 kcal mol^{-1} at $r_{C_\alpha O} = 2.1$ Å, a distance large enough so the C_αO covalent bond is still not formed. Inside the well, the electronic wavefunction exhibits a strong superoxide (O_2^-) character, and it seems that the well is stabilized by a strong charge-dipole interaction. The singlet and the triplet states cross at the bottom of the well, which coincides with the MECP. The second minimum is significantly deeper (just 3.4 kcal mol^{-1} higher than the minimum of the triplet state)

and is located at $r_{C_\alpha O} = 1.4$ Å. This minimum is associated with the peroxide formation.

The two minima are separated by a maximum on the one-dimension curve, which corresponds to a saddle-point. It lies slightly below the asymptotic energy of the 1^1[DPA-O_2] state. This saddle-point is associated with the barrier of the superoxide to peroxide transformation and arises from an avoided crossing. The huge gap in energy between states at the saddle-point indicates that the non-adiabatic couplings are very strong in this region, suggesting that the charge transfer may occur adiabatically. We should point out that the barrier height predicted by our method is probably overestimated, partially because of the constraints imposed to keep the structure planar and also, as we will discuss later, owing to the small size of the active space. The planar restraint imposed on butenthioate also affects the relative energy of the minimum of the first singlet and triplet states and causes the 1^1[DPA-O_2] minimum to lie above the minimum energy 1^3[DPA-O_2] state. It should be noticed that this does not affect the energy profile for $r_{C_\alpha O} > 2$ Å, where the peroxide bond is not formed, and the molecule is intrinsically planar. Thus, the MECP region should not be affected by the planar restraint.

To get more insight into the nature of the states that are involved in the intersystem crossing, we generated the quasi-diabatic states for the addition of O_2 to butenthioate. Diabatic curves are not appropriate to track the position of MECP, as diabatic energies do not include the couplings between the states, which, in the diabatic representation, are included in the non-diagonal elements of the electronic Hamiltonian matrix. However, quasi-diabatic states retain the character displayed at asymptotic distances, making it possible to extend the assignment of an electronic configuration for independent O_2 and butenthioate to small C_α–O distances. Diabatic states are calculated as a function of $r_{C_\alpha O}$ for three different C_α-O-O angles: 110°, which is close to the value obtained for the fully relaxed geometries shown in Figure 3; 180° for which O_2 inserts perpendicular to the butenthioate plane and minimizes the overlap between $(p_{C\alpha})$ and $(\pi_{O_2}{}^*)$ orbitals; and 150°, an intermediate value in order to see the evolution. In the left panels of Figure 4 we show the adiabatic curves of the ap-

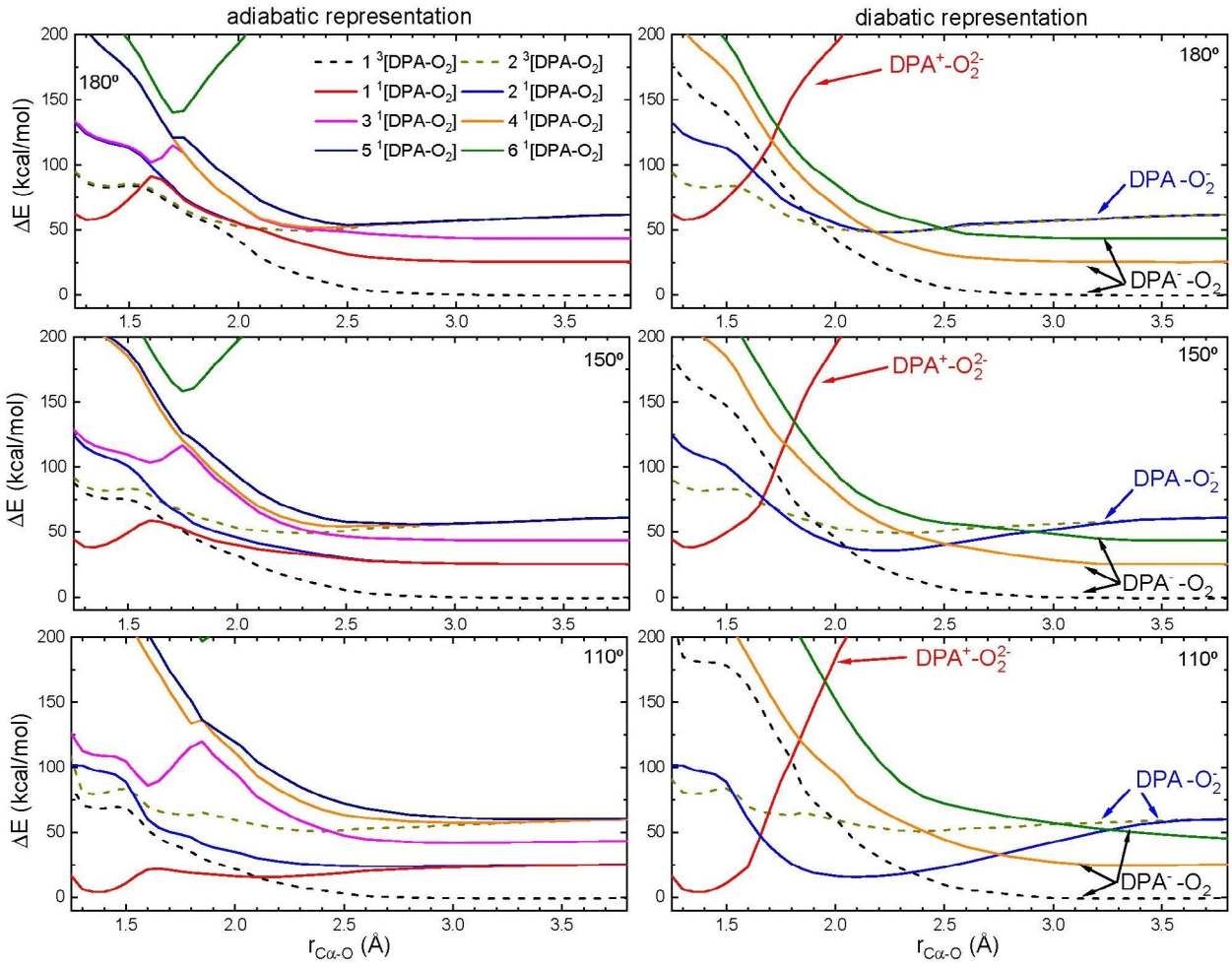

Figure 4. Energy profiles for the addition of O_2 to *S*-methyl-but-3-enethioate as a function of the C_α–O distance and the C_α-O-O angle. In the left panels, the adiabatic curves are shown and their corresponding diabatic curves are shown in the right panels. C_α-O-O = 110° corresponds to the minimum energy at the MECP shown in Figure 3. The curves for the singlet (triplet) states are shown in solid (dashed) lines. Calculations carried out at the MRCI(4,3)/6-31 + G(d,p) level of theory.

proaching of O_2 to butenthioate, whereas the diabatic states are shown in the right panels.

In the absence of overlap between $(p_{C\alpha})$ and $(\pi_{O_2}{}^*)$ orbitals, C_α-O-O = 180°, only the 6^1[DPA-O_2] adiabatic state is not repulsive for $r_{C_\alpha O} > 2$ Å. As non-adiabatic couplings are small for this orientation, diabatic and adiabatic representations are very similar. At C_α-O-O = 180°, 1–2^1[DPA-O_2] as well as 4–5^1[DPA-O_2] adiabatic states are nearly degenerate for distances down to 1.7 Å. For this orientation and $r_{C_\alpha O} = 1.4$ Å, we observe a shallow minimum on the first singlet state. The quasi-diabatization procedure reveals unambiguously that this minimum correlates to the 6^1[DPA-O_2] ionic state, and it is associated with a DPA$^+$-O_2^{2-} (peroxide) conformation.

When the orientation deviates from C_α-O-O = 180°, $(p_{C\alpha})$ and $(\pi_{O_2}{}^*)$ orbitals mix, non-adiabatic couplings get stronger, and the degeneracy between 1–2^1[DPA-O_2] and 4–5^1[DPA-O_2] breaks again. It is worth noticing that with the increasing strength of the non-adiabatic couplings, the adiabatic picture deviates progressively from the diabatic view, implying that couplings affect several states simultaneously.

Using the diabatic representation, we can establish that the peroxide minimum is associated with DPA$^+$-O_2^{2-}, as expected. The diabatization also permits us to assign the first minimum of the first singlet state, around the MECP, to the well associated with a DPA-O_2^- state. This finding is confirmed by the coefficients of the CI vector displayed in Figure S2 (in the Supporting Information).

The mechanism that emerges from these results is the following: O_2 addition starts with a first charge transfer between butenthioate and O_2, leading to the formation of the superoxide anion. This charge transfer is concomitant with intersystem crossing and is therefore mediated by the strength of SOC in this region. Following this process, a second charge transfer step takes place, between two singlet states, and leads to the formation of the peroxide.

In the above discussion we have assumed that the electron is transferred "at once". However, this classical picture is not fully correct because, although the dominant character in the well is the one of the superoxide, both DPA-O_2^- and DPA$^-$-O_2 states are coupled and strongly mixed. It is therefore more accurate to discuss about the transference of electronic density. To account for this effect, Figure S3 (in the Supporting Information) shows the evolution of the partial charge, which is accumulated on the O_2 moiety as a function of $r_{C_\alpha O}$. As can be observed, spin flipping is associated with an appreciable electron density transfer from buthentioate to O_2, although part of the electronic density had been already transferred to O_2 before the intersystem crossing.

The nature of the two states involved in the spin-change process has important implications for the feasibility of the process. According to El-Sayed rules, if the change of spin is associated with a change in the orbital angular momentum (or electronic configuration), the spin-orbit coupling would be strong, and the rate coefficient of the spin-forbidden process would be large,[61] even if there is only a small change in electronic density.[62] The values of the SOC between the ground triplet state and the six singlet states are shown in Figure 5. At large $r_{C_\alpha O}$ distances, only the SOC with the 3^1[DPA-O_2] ($^1\Sigma_g^+$ of O_2) is large, as was observed for isolated O_2.[63,64] When O_2 and butenthioate approach, the value of the SOC between the first singlet and triplet states increases smoothly with the energy, which could be explained by the transfer of electronic density from butenthioate to O_2 (and the higher weight of the O_2^- states in the CI vector of the first singlet state, as shown in Figure S2 in the Supporting Information). The SOC reaches a plateau value of 75 cm^{-1} in the region of the MECP, in accordance with the estimated value of 76.5 cm^{-1} based on O_2^- spectroscopic assignments.[31,33] This value of SOC is strong enough to promote intersystem crossing, even in the absence of any metal cofactor.

Larger SOC values are typically associated with the presence of heavy atoms. To check the role of the S-CH_3 group, SOCs were calculated by replacing S with O. As a result, similar values of SOC were obtained, concluding that S does not influence the SOC, and that the values of SOC obtained for this system should be similar for other cofactorless spin-forbidden reactions between O_2 and enolates.

To get more insight into the geometry of the crossing seam (the region in which singlet and triplet states are degenerate), Figure 6 displays energy contour plots for the approach of O_2 to butenthioate as a function of both $r_{C_\alpha O}$ and $\varphi(C_\beta$-C_α-O-O), the dihedral angle between C_β-C_α-O-O for the first singlet and triplet states (C_β is defined in Figure 2). For the triplet state, the energy barely depends on $\varphi(C_\beta$-C_α-O-O), and the curve is purely repulsive (as expected from Figure 3). On the other hand, the PES of the first singlet state is considerably anisotropic. The first well, that associated to DPA-O_2^-, is located at $r_{C_\alpha O} = 2.1$ Å, and $\varphi(C_\beta$-C_α-O-O) ≈ 210°. A second shallower minimum is found at $\varphi(C_\beta$-C_α-O-O) ≈ 60°, when the O_2 is closer to S than to the C=C double bond. The absolute minimum is associated with the DPA$^+$-O_2^{2-} configuration, and is reached at

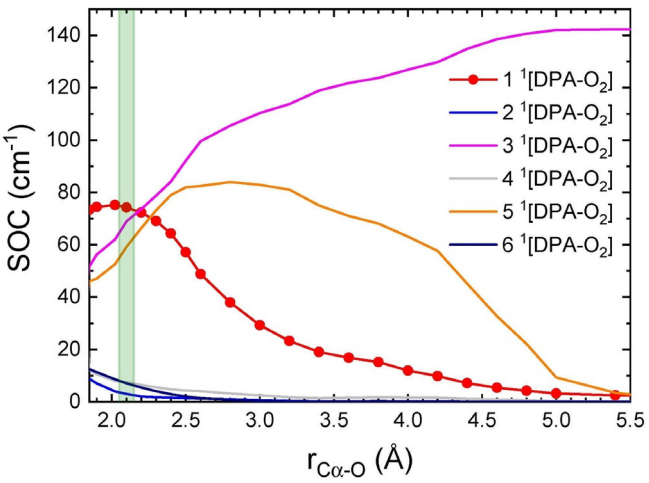

Figure 5. Values of the Spin-Orbit Coupling (SOC) between the ground triplet state and the six singlets involved in the oxidation of DPA-CoA as a function of the C_α–O distance. The values of the SOC between the ground singlet and triplet states are shown as red, closed circles. The region in which the MECP was found is shaded in green. Calculations carried out at the MRCI(4,3)/6-31+G(d,p) level of theory.

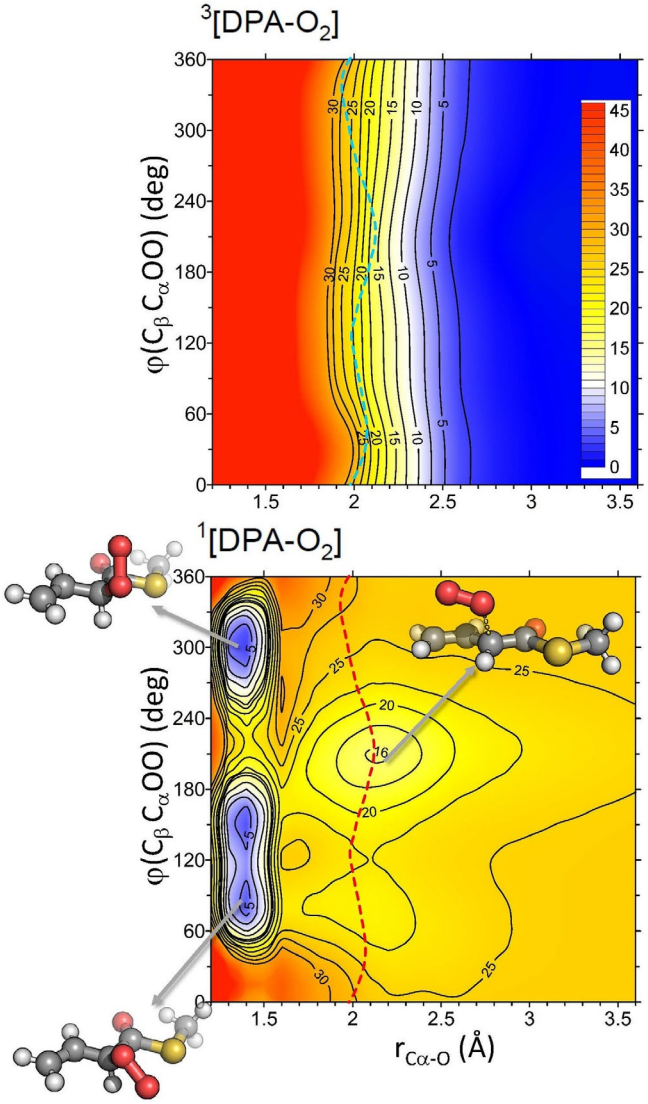

Figure 6. 3D contour map of the energy profile for the addition of O_2 to *S*-methyl-but-3-enethioate as a function of C_α–O distance and the C_β-C_α-O-O dihedral angle. Top panel: Lowest triplet state. Bottom panel: Lowest singlet state. The crossing seam is shown as a dashed line on top of the contour maps. The geometry of the MECP and two of the peroxide minima are shown. Energies are in kcal mol^{-1}. Calculations carried out at the MRCI(4,3)/6-31+G(d,p) level of theory.

$r_{C_\alpha O} = 1.4$ Å for three different values of $\varphi(C_\beta\text{-}C_\alpha\text{-O-O})$. The crossing seam is represented by the dashed line on top of the contour maps. Regardless of the value of $\varphi(C_\beta\text{-}C_\alpha\text{-O-O})$, the seam is found for $2\text{ Å} < r_{C_\alpha O} < 2.1$ Å, where the triplet PES crosses the singlet PES at the DPA-O_2^- minimum.

The geometries of the MECP and two of the absolute minima are also depicted in Figure 6. The carbon scaffold of butenthioate was restrained to be planar and, at the MECP, the bond between H and C_α nearly lies in the butenthioate plane, suggesting that C_α still presents a sp^2 hybridization, and that the aromatic cloud is not yet perturbed by the O_2 approach. The O–O distance is 1.29 Å, closer to that observed for O_2^- (1.345 Å) than for O_2 (1.215 Å).[65] At smaller values of $r_{C_\alpha O}$, the hydrogen progressively folds out of the plane while the $C_\alpha O$ bond is formed, as expected for a sp^3 hybridization of C_α.

To study the effect of increasing considerably the number of active orbitals, we recalculated the energy profile for the addition of O_2 to butenethioate by using the Semistochastic Heat-Bath Configuration Interaction (SHCI) method.[66–68] SHCI is a recently developed semistochastic method, which permits us to circumvent the limitation in the number of orbitals of the active space, and can account for dynamic correlations by perturbation theory. For the SHCI calculations, the active space was formed by 23 orbitals, including the p_z orbitals of the sp^2 C and the 2p and 3d orbitals of O_2 (the 23 orbitals are shown in Figure S4 in the Supporting Information). The results using SHCI are shown in Figure 7 and are in qualitative agreement with the MRCI calculations, with the main differences being the much lower barrier between the superoxide and peroxide region, and the larger stability of the peroxide. The energy height of the MECP, however, is very similar to that obtained by using MRCI. In Figure 7, we also show the SHCI results obtained when the 3d orbitals of O_2 were not included. In this case, there is a huge barrier that prevents intersystem crossing. It clearly shows that the SHCI results strongly depend on the number of orbitals of the active space, which let us believe that the MRCI barrier between peroxide and superoxide would be significantly smaller if calculations could be carried out including a very large active space that also includes the 3d orbitals of O_2.

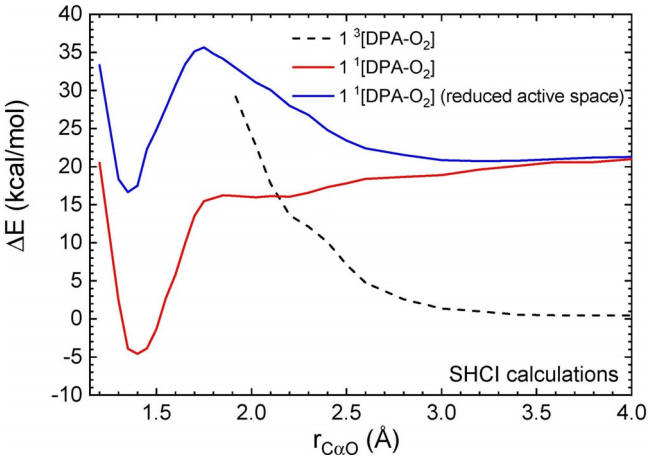

Figure 7. Energy profile for the addition of O_2 to *S*-methyl-but-3-enethioate as a function of the C_α–O distance by using SHCI method, a 6-31+G(d,p) basis set, and a (18,23) active space. The solid blue curve shows the results obtained for the singlet state when the 3d orbitals of O_2 have been excluded from the active site.

2.2. Reaction between O_2 and DPA-CoA in DpgC

Once we have described the nature of the electronic states involved in the process, and how intersystem crossing takes place in our model system, we studied the addition of O_2 to DPA-CoA catalyzed by DpgC, which is likely to be the rate-limiting step for the formation of DPGX (Figure 1) using QM/MM calculations. Owing to the larger system size of the QM region

(see bottom panel of Figure 2), we cannot go beyond DFT calculations. This impedes the calculation of all the relevant electronic states, but allows us to determine the role of the protein environment and to study the possible proton transfer mechanisms.

To analyze the mechanism of this reaction, we carried out restrained geometry optimizations by using $\Delta E^{Sing/Trip}$, the energy difference between the first singlet and triplet states, as a reaction coordinate. This selection has two important advantages: i) the MECP is localized exactly at $\Delta E^{Sing/Trip}=0$, and ii) the evolution from the triplet to the singlet state is smoother.

The QM/MM energy profile for the O_2 addition to DPA-CoA is shown in Figure 8. QM/MM results show that both the triplet and the singlet states show only one minimum, which is very broad for the case of the singlet state. Interestingly, we observe that the MECP is the only barrier for the reaction, and accordingly should act as the dynamic bottleneck. MECP lies 16.7 kcal mol^{-1} above the minimum for the triplet state, in very good agreement with the value obtained for the O_2–butenthioate model. The formation of the peroxide is driven by an exothermicity of 9.9 kcal mol^{-1}.

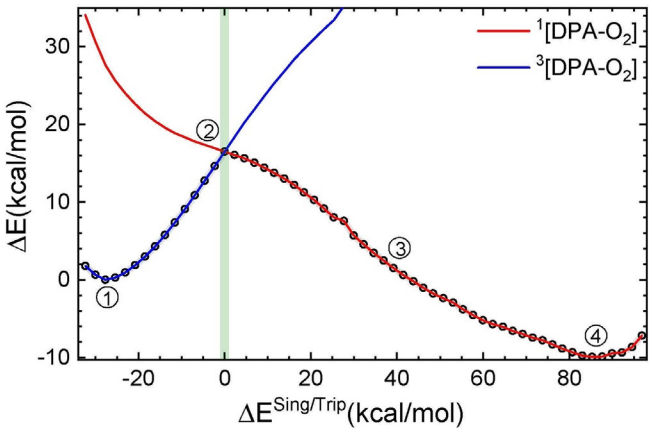

Figure 8. QM/MM energy profile for the addition of O_2 to the DPA model as a function of the energy difference between the ground singlet and triplet states. $\Delta E^{Sing/Trip}=0$ corresponds to the MECP, and it is shaded in green. The framed numbers highlight the values of $\Delta E^{Sing/Trip}$ corresponding to the structures shown in Figure 9. Calculations carried out at the B3LYP/6-31+G(d,p) level of theory.

To investigate the effect of the protein in the QM/MM energy profile, we repeated the calculations using a reduced QM region, in which Ile324, Gln299, Ala319, and one of the water molecules were excluded from the QM region. The obtained results were pretty similar, except for the exothermicity, which is somewhat smaller (5.6 kcal mol^{-1}), evidencing that the protein scaffold plays only a minor role in the promotion of the intersystem crossing beside the stabilization of the enolate (results are not shown).

The structures of the minimum of the triplet state, the MECP, the point at $\Delta E^{Sing/Trip}=39$ kcal mol^{-1}, and the minimum of the singlet state are depicted in Figure 9. The structure obtained for the triplet state minimum is very similar to the crystal structure, although in this case O_2 has moved slightly closer to C_α. Indeed, the position of the two water molecules that are close to O_2 and C_α is very similar in the crystal. Regarding these water molecules, it could have been expected that one of the water molecules could protonate the triplet O_2 as was predicted for the reaction between O_2 and flavin.[28,30,33] However, at the MECP, the proton is still on the water. In fact, the main differences between the minimum associated with the triplet and the MECP are that the hydrogen bound to C_α has moved slightly below the plane formed by the π system of DPA, and that O_2 is significantly closer to C_α. This is shown in Figure 10, where we display the evolution of the C_α–O, and the O–O distances along the reaction path. In the figure, we also show the progress of the proton transfer, which is defined as the difference between the r_{H-OH} and the r_{O-H_2O} (as defined in Figure 9).

Between the triplet minimum and the MECP, $r_{C_\alpha O}$ has changed from 3.2 to 2 Å, in excellent agreement with the results obtained for the butenthioate model. Based on these results, the first triplet state is purely repulsive, so we can predict that systems for which $r_{C_\alpha O}$ is larger (smaller) at the MECP will be more (less) reactive.

After the MECP, $r_{C_\alpha O}$ decreases slowly, and only reaches its equilibrium value of 1.4 Å for $\Delta E^{Sing/Trip}>45$ kcal mol^{-1}. Interestingly, at $\Delta E^{Sing/Trip}=39$ kcal mol^{-1}, the structure resembles that obtained for the MECP with the sole exception that the C_α–O bond is formed. Still, the proton has not been transferred to the peroxide. This means that proton transfer occurs significantly after the peroxide is formed. Probably, that is the reason why there are not basic residues around the active site that could donate a proton to O_2, as was observed for other cofactorless reactions.[28,30,33] Proton transfer drifts the system away from the MECP and, even in the minimum associated with the singlet state, the proton is only shared between the peroxide and the water.

In the minimum of the singlet state, the water wire that connects the bulk to the active site has reorganized. In particular, the water molecule that connects Gln299 and C_α is reoriented to a position suitable for the extraction of the C_α proton, which would facilitate the following step in DPGX formation. This water molecule was resolved in the crystal structure and was not exchanged with the solvent throughout the MD simulations.

Combining the height of the MECP obtained in the QM/MM calculations, with the SOC obtained using our model, and plugging them in the Landau–Zenner equation,[45,50] we could estimate k_{cat}. We obtained a hopping probability of 0.06, which is equivalent to an increase of 1.6 kcal mol^{-1} in the activation energy at 300 K. By using these values, we obtain a $k_{cat}=0.23$ s^{-1}, very close to the experimental value of 0.15 s^{-1}.[43] The quantitative agreement between the experiment and the simulation is coincidental, considering the approximations used. However, it supports the validity of the mechanism proposed in this article for intersystem crossing and subsequent formation of the peroxide.

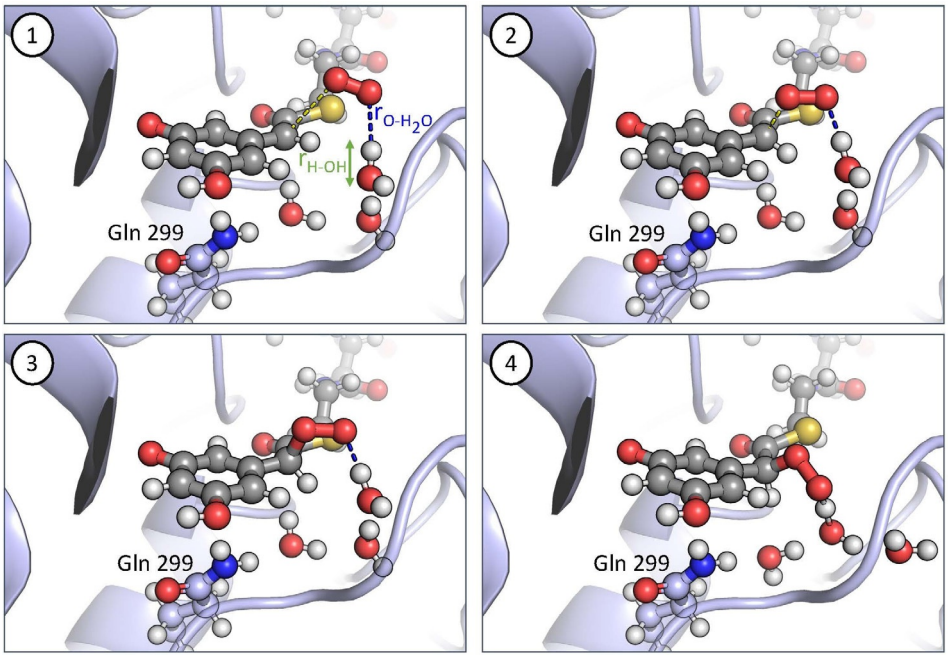

Figure 9. QM/MM structures along the $\Delta E^{Sing/Trip}$ path. 1) Structure corresponding to the optimized triplet geometry. 2) Structure of the system at the MECP. 3) Structure of the system for $\Delta E^{Sing/Trip} \approx 40$ kcal mol^{-1}. 4) Structure of the optimized singlet structure. C_α–O, H–OH, and O–H_2O distances are shown in yellow, green, and blue. Gln299, three water molecules that are included in the QM region, DPA-CoA, and O_2 are shown atomistically.

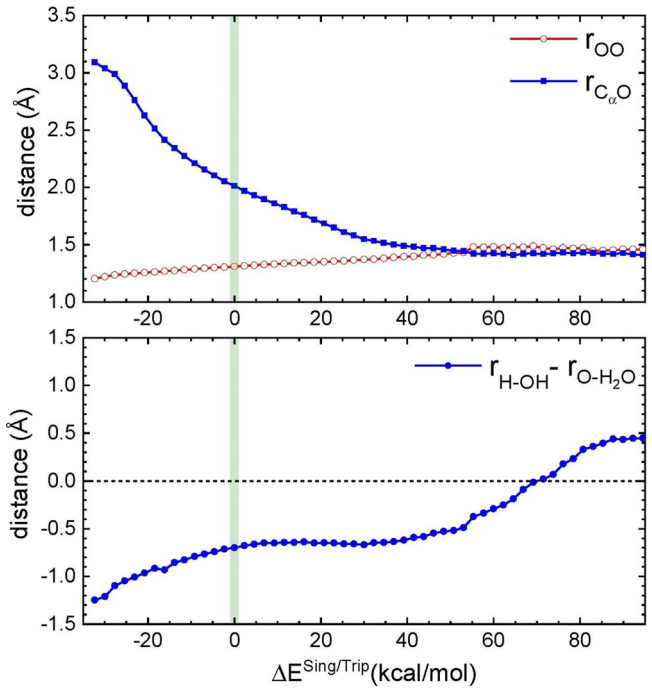

Figure 10. Evolution of the O–O, C_α–O, and proton transfer coordinate (defined as $r_{H-OH} - r_{O-H_2O}$) along the $\Delta E^{Sing/Trip}$ path. $\Delta E^{Sing/Trip} = 0$ corresponds to the MECP, and it is shaded in green. Calculations carried out at the B3LYP/6-31 + G(d,p) level of theory.

3. Conclusion

Incorporation of molecular oxygen into an organic substrate involves a change in the spin state of the system, that is, proceeds through intersystem crossing. To catalyze these reactions, enzymes typically require metal cofactors, generally iron. Intriguingly, a subgroup of oxygenases performs these reactions without the presence of any cofactor. Here, we have investigated the mechanism of this spin-forbidden process by using MRCI quantum calculations and QM/MM simulations on the reaction between DPA-CoA and O_2 catalyzed by DpgC. By using MRCI calculations, we calculated the potential energy surfaces of the nine concurrent electronic states on an equal footing, and assigned an electronic configuration to each of them through a diabatization procedure. Our results provide evidence that, once the enolate is formed, the reaction can occur without any previous activation of O_2 and via two successive electron transfer processes. The minimum energy crossing point (MECP), which plays the role of an effective barrier for spin-forbidden processes, lies only 16.7 kcal mol^{-1} above the DPA-CoA + $^3O_2$ asymptote, which is compatible with the experimental k_{cat} value.

Intersystem crossing occurs between the triplet state that correlates to DPA^--O_2 and the singlet state that correlates diabatically with a DPA-O_2^- state, that is, it is associated to the charge transfer from DPA to O_2 to form a superoxide anion. As this change of spin is associated with a change in the electronic configuration, it complies with the El-Sayed rules, and the strength of the spin-orbit coupling is above 70 cm^{-1}, a relatively large value for a system that does not include heavy atoms.

For other spin-forbidden processes, it has been postulated that the rate for the spin-forbidden reaction is enhanced by the presence of a broad crossing region, which maximizes the cross-over probability. That is not the case for the reaction between DPA-CoA and O_2, for which this probability is maximized by the presence of a stable intermolecular complex arising from the charge-dipole interaction, which stabilizes the superoxide singlet state, lowering the energy of the MECP. For the formation of peroxide, a second charge transfer from DPA to O_2 is required.

Our QM/MM calculations reveal that the minimum energy crossing point is the main reaction bottleneck. They also suggest that protonation of O_2 takes place after the formation of the peroxide, which is already stable in its deprotonated form. This could explain the absence of basic residues in the active site that could protonate O_2 during its addition to the enolate. It is also relevant that the first molecule of the water wire that connects the active site to the bulk changes its orientation following the formation of the peroxide. In their final configuration, it could easily capture the proton, which could initiate the following step in the formation of DPGX. Finally, the comparison between the energy profiles calculated by using different QM regions suggests that although the protein environment plays an important role in the diffusion of O_2 towards the active site, and in the formation and stabilization of the enolate, it plays a passive role in the promotion of the spin-forbidden reaction. We believe that these results are general and that similar behavior should be observed for other cofactorless spin-forbidden reactions that proceed via the formation of a peroxide.

4. Experimental Section

4.1. Initial coordinates and molecular dynamics simulations

The initial structure adopted in this work is based on the crystal structure of the DpgC/DPA-NH-CoA/O_2 complex (PDB: 5KAG, 2.68 Å resolution).[38] That crystal structure was obtained by replacing the original substrate (DPA-CoA, see Figure 1) by the stable substrate analog (DPA-NH-CoA) to prevent the reaction even in aerobic conditions. This structure corrected the crystallographic pathologies of the original crystal structure,[36] (PDB: 2NP9) caused by a wrong assignment of the crystal lattice. In our simulations, we exchanged DPA-NH-CoA with DPA-CoA while keeping O_2 in its crystallographic position, a hydrophobic pocket less than 4 Å away from C_α of DPA, and the initial geometry was prepared by using CHARMM-GUI.[69,70] Hydrogen coordinates were generated with standard protonation states for all titrable residues by using CHARMM,[71] and the protein complex was placed in the center of a cubic TIP3 water box large enough to include the protein and at least 10 Å of solvent on all sides. Additionally, water molecules were randomly replaced by K^+ and Cl^- ions to ensure the neutralization of the system, and provide an additional concentration of 0.15 M KCl. The system was subject to a classical MD equilibration of 10 ns at constant temperature ($T = 303.15$ K) and pressure (1 atm) by using NAMD (http://www.ks.uiuc.edu/Research/namd/),[72] and CHARMM-36m forcefield.[73,74] The Particle Mesh Ewald method was used for the electrostatics of the periodic boundary conditions.[75] A time step of 2 fs was used with the ShakeH algorithm.[76] To avoid O_2 diffusion outside the active site, the positions of O_2 and the non-hydrogen atoms of DpgC were fixed throughout the equilibration. The root-mean-square deviation (RMSD) with respect to the initial conformation was calculated for all the non-hydrogen protein atoms, which were not located in any turn or coil (see Figure S5 in the Supporting Information) showing that the structure was well converged after 4 ns, with an average RMSD of 1.56 Å.

To select an initial frame for the subsequent QM/MM calculations, we calculated the occupancy of water molecules in the active site by following the same procedure used in ref. [77]. Considering the last 5 ns of the MD trajectory, we calculated the averaged position of the water molecules within 7 Å of the O_2 molecule, and selected a frame for which the position of the waters was close to their average position. Compared with the initial structure, the two water molecules crystallized around the active site kept their positions (although one of them exchanged with the solvent during the simulation time), whereas the active site recruited a third water molecule and a water wire connecting the active site and the bulk was formed. A representation of the initial structure for QM/MM calculations is shown in Figure S6 (in the Supporting Information).

4.2. QM/MM calculations

Once the system was classically equilibrated and the initial frame was selected, it was trimmed to a sphere of 26 Å centered at the S atom of DPA-CoA. Atoms further away than 18 Å from the S atom of DPA-CoA were kept frozen during all the QM/MM calculations. A full electrostatic embedding[78] was adopted in all the calculations, using hydrogen link atoms to treat the QM/MM boundaries, maintaining the effect of the broken chemical bond between the QM and the MM region. QM/MM calculations were run coupling Q-Chem v5.2[79] and CHARMM.[71] QM calculations were carried out at the B3LYP/6-31G+(d,p) DFT level of theory for the ground singlet and triplet states. The D3 version of Grimme's dispersion correction was used.[80,81]

Initial optimization of the reactants ($DPA^- + O_2$) and products (DPA-OO^-) confirmed that the reactants were only stable in their triplet state, whereas the peroxide was only stable as a singlet. It also revealed that the protein prevents the bending of the DPA-OO^- peroxide, which remains almost planar. The reaction path was scanned by performing restrained geometry optimizations along a reaction coordinate, which was defined as the energy difference between the ground triplet and singlet state, $\Delta E^{\mathrm{Sing/Trip}} = E^{\mathrm{triplet}} - E^{\mathrm{singlet}}$, so the crossing seam is found for $\Delta E^{\mathrm{Sing/Trip}} = 0$. To impose that restraint, we added the following harmonic term to the potential:

$$V = V_0 + \frac{1}{2}K\left(\Delta E^{\mathrm{Sing/Trip}} - \Delta E_i^{\mathrm{Sing/Trip}}\right)^2 \quad (1)$$

where V_0 is the minimum value between E^{triplet} and E^{singlet}, K is the spring constant (the value of which was set to 500 eV^{-1}), $\Delta E_i^{\mathrm{Sing/Trip}}$ is the reference value of $\Delta E^{\mathrm{Sing/Trip}}$ to which the potential is biased, and V is the resulting biased potential energy. More details for the MECP search algorithm for QM/MM calculations are given in the extended methods section in the Supporting Information.

4.3. Multireference calculations

4.3.1. MRCI calculations

The reaction between *S*-methyl-but-3-enethioate and O_2 was simulated by using the multiconfiguration reference internally contracted configuration interaction method (MRCI), which captures the static correlation by the selection of all the electronic configura-

tions that can be generated by the distribution of the electrons considered in the orbitals that belong to the active space. The dynamic correlation is then captured by optimizing variationally the best solution of a linear combination of all the electronic configurations generated by simple and double electronic excitations from all the reference configurations generated by the active space towards the orbitals of the virtual space. To account for the quadruple excitations and reduce the size-consistency error inherent to the method, Davidson correction has been applied.

Calculations were carried out by using the MOLPRO package,[82] and a 6-31G+(d,p) basis set. For efficiency reasons, the geometries were first optimized at a DFT level using the B3LYP functional, and the D3 version of Grimme's dispersion correction, following by single-point MRCI calculations. This procedure is similar to the approach employed to shed light on the reactivity of metallic clusters.[83,84] The only difference is that here, the MECP was also optimized.

The procedure applied here is the following: first, the MECP between triplet and singlet was optimized at the DFT level. Then, starting from that structure, the geometry was relaxed for different values of the reaction coordinate, which we assimilated to C_α–O distance ($r_{C_\alpha O}$). $r_{C_\alpha O}$ was sampled from 1.2 to 7 Å, and taking as a reference value the $r_{C_\alpha O}$ distance at the MECP, for larger (smaller) $r_{C_\alpha O}$ values the geometry was optimized in its triplet (singlet) state. Furthermore, it allows a double-check to confirm that the electronic wavefunctions converge to the correct state, which is particularly tedious in the case of O_2.

The energy of the geometries obtained at DFT level was recalculated by using the internally contracted version of MRCI available in MOLPRO.[85,86] Within this method, SOC can be calculated rigorously by using the Breit–Pauli spin-orbit operator. The first step required before running MRCI calculations is the definition of the initial wavefunction. In this work, the guess wavefunction was generated through a state-average CASSCF calculation[87,88] including in the active space four electrons in three orbitals: the two π_g^* orbitals of O_2 and the HOMO of *S*-methyl-but-3-enethioate. In the state-average CASSCF wavefunction, one triplet and five singlet states were treated on an equal footing. This approach leads to stable optimized orbitals and configurations along the reaction path, which is required to obtain accurate and meaningful potential energy curves at a multireference level, which is hard to achieve for relatively large polyatomic systems. For the subsequent MRCI calculation, we computed the nine states (three triplet and six singlet states) and the SOC between them. Under these conditions, the electronic wavefunctions of the triplet (singlets) states are constructed over a linear combination of about 6×10^6 (30×10^6) contracted configurations.

To check how the results change when a larger active space is used, we compared the calculations using the (4,3) active space with those including ten electrons in seven orbitals. The relative energies for the two active spaces are similar (see Figure S7 in the Supporting Information) with MRCI(10,7) predicting a shallower peroxide well for the first singlet state. In fact, PESs are more sensitive to the number of states included in the MRCI treatment.

Owing to the relatively large number of coupled electronic states, avoided crossings in the adiabatic potential energy curves may impair their interpretation. In these cases, it may be useful to calculate the states in the diabatic representation, which also sheds light on the nature of the electronic states involved. As we are considering singlet and triplet states simultaneously, an automatic diabatization algorithm cannot be employed, so we applied the diabatization model based on the geometrically based approach,[89] which has been successfully applied to diabatize highly entangled excited states of alkyl radicals.[90–92] It consists of a geometric approach where successive 2×2 diabatizations are performed between all coupled states iteratively. The validity of the approach was confirmed by the comparison between our diabatic curves and those obtained by using the default MOLPRO algorithm for the three triplet states (see Figure S8 in the Supporting Information). More details about the diabatization method can be found in the extended methods section in the Supporting Information.

4.3.2. Semistochastic heat-bath configuration interaction

The reaction between *S*-methyl-but-3-enethioate and O_2 was also simulated by using the recent Semistochastic Heat-Bath Configuration Interaction (SHCI) method,[66–68] which permits us to overcome the critical limitation to the maximum number of orbitals that can be included in a multiconfigurational self-consistent field (MCSCF) calculation (depending on the system, up to 14–18 orbitals).

The SHCI algorithm consists of two stages. First, a variational wavefunction is computed by using a set of iteratively selected determinants. These determinants are stochastically sampled, and they are filtered under a chosen energy value threshold (ε_1). The algorithm increases the number of determinants included in the set until the wavefunction has constant and stable energy. In the second stage, the second-order correction to the variational energy is computed by using the multireference Epstein–Nesbet perturbation theory.

The resulting energy is considered to be Full-Configuration Interaction (FCI) for a given active apace and basis set. To obtain the FCI energy, several calculations are computed for different values of ε_1 and they are extrapolated to $\varepsilon_1\rightarrow0$. All the SHCI calculations were done in the open-source Python software package PySCF,[93] interfaced with the fast version of the algorithm, Arrow.[94]

Acknowledgements

The authors thank Prof. Enrique Verdasco for his support and help with the calculations. Funding by the Spanish Ministry of Science and Innovation (grants PGC2018-096444-B-I00, and FIS2017-83473-C2-2-P) is also acknowledged. The authors acknowledge funding by Fundación Salamanca City of Culture and Knowledge (Programme for Attracting Scientific Talent to Salamanca).

Conflict of interest

The authors declare no conflict of interest.

Keywords: charge transfer mechanism · cofactor-independent enzymes · oxidation · oxygenases · spin-forbidden transitions

[1] H. D. Holland, *Philos. Trans. R. Soc. B* **2006**, *361*, 903–915.
[2] R. Ligrone, *The Great Oxygenation Event*, Springer International Publishing, Cham, **2019**, pp. 129–154.
[3] C. W. Machan, *ACS Catal.* **2020**, *10*, 2640–2655.
[4] M. L. Pegis, C. F. Wise, D. J. Martin, J. M. Mayer, *Chem. Rev.* **2018**, *118*, 2340–2391.
[5] C. Feng, M. B. Faheem, J. Fu, Y. Xiao, C. Li, Y. Li, *ACS Catal.* **2020**, *10*, 2019–4047.
[6] T. D. H. Bugg, *Tetrahedron* **2003**, *59*, 7075–7101.
[7] S. Sahu, D. P. Goldberg, *J. Am. Chem. Soc.* **2016**, *138*, 11410–11428.
[8] A. J. Jasniewski, L. Que, *Chem. Rev.* **2018**, *118*, 2554–2592.
[9] W. Zhang, W. Lai, R. Cao, *Chem. Rev.* **2017**, *117*, 3717–3797.

[10] C. E. Elwell, N. L. Gagnon, B. D. Neisen, D. Dhar, A. D. Spaeth, G. M. Yee, W. B. Tolman, *Chem. Rev.* **2017**, *117*, 2059 – 2107.
[11] M. Wikström, K. Krab, V. Sharma, *Chem. Rev.* **2018**, *118*, 2469 – 2490.
[12] E. C. Kisgeropoulos, J. J. Griese, Z. R. Smith, R. M. M. Branca, C. R. Schneider, M. Högbom, H. S. Shafaat, *J. Am. Chem. Soc.* **2020**, *142*, 5338 – 5354.
[13] S. S. Chaturvedi, R. Ramanan, N. Lehnert, C. J. Schofield, T. G. Karabencheva-Christova, C. Z. Christov, *ACS Catal.* **2020**, *10*, 1195 – 1209.
[14] R. Suardíaz, P. G. Jambrina, L. Masgrau, A. González-Lafont, E. Rosta, J. M. Lluch, *J. Chem. Theory Comput.* **2016**, *12*, 2079 – 2090.
[15] K. P. Jensen, U. Ryde, *J. Biol. Chem.* **2004**, *279*, 14561 – 14569.
[16] A. Cebrián-Prats, A. Gonz'alez-Lafont, J. M. Lluch, *ACS Catal.* **2020**, *10*, 138 – 153.
[17] C. M. Marian, *WIREs Comput. Mol. Sci.* **2012**, *2*, 187 – 203.
[18] G. Baryshnikov, B. Minaev, H. Agren, *Chem. Rev.* **2017**, *117*, 6500 – 6537.
[19] P. Chaiyen, M. W. Fraaije, A. Mattev, *Trends Biochem. Sci.* **2012**, *37*, 373 – 380.
[20] A. Mattevi, *Trends Biochem. Sci.* **2006**, *31*, 276 – 283.
[21] E. Romero, J. R. Gomez Castellanos, G. Gadda, M. W. Fraaije, A. Mattevi, *Chem. Rev.* **2018**, *118*, 1742 – 1769.
[22] S. Thierbach, N. Bui, J. Zapp, S. R. Chhabra, R. Kappl, S. Fetzner, *Chem. Biol.* **2014**, *21*, 217 – 225.
[23] S. Bui, R. A. Steiner, *Curr. Opin. Struct. Biol.* **2016**, *41*, 109 – 118.
[24] X. Fetzner, R. A. Steiner, *Appl. Microbiol. Biotechnol.* **2010**, *86*, 791 – 804.
[25] L. Gabison, C. Chopard, N. Colloc'h, F. Peyrot, B. Castro, M. El Hajji, M. Altarsha, G. Monard, M. Chiadmi, T. Prang'e, *Proteins* **2011**, *79*, 1964 – 1976.
[26] D. Wei, X. Huang, Y. Qiao, J. Rao, L. Wang, F. Liao, C.-G. Zhan, *ACS Catal.* **2017**, *7*, 4623 – 4636.
[27] S. Bui, D. von Stetten, P. G. Jambrina, T. Prange, N. Colloc'h, D. de Sanctis, A. Royant, E. Rosta, R. A. Steiner, *Angew. Chem. Int. Ed.* **2014**, *53*, 13710 – 13714; *Angew. Chem.* **2014**, *126*, 13930 – 13934.
[28] S. Visitsatthawong, P. Chenprakhon, P. Chaiyen, P. Surawatanawong, *J. Am. Chem. Soc.* **2015**, *137*, 9363 – 9374.
[29] P. J. Silva, *PeerJ* **2016**, *4*, e2805.
[30] F. G. Cantú Reinhard, J. L. DuBois, S. P. de Visser, *J. Phys. Chem. B* **2018**, *122*, 10841 – 10854.
[31] B. F. Minaev, *Chem. Phys.* **2019**, *521*, 61 – 68.
[32] R. Prabhakar, P. E. M. Siegbahn, B. F. Minaev, *Biochim. Biophys. Acta Proteins Proteomics* **2003**, *1647*, 173 – 178.
[33] R. Prabhakar, P. E. M. Siegbahn, B. F. Minaev, H. Agren, *J. Phys. Chem. B* **2002**, *106*, 3742 – 3750.
[34] M. M. Machovina, R. J. Usselman, J. L. DuBois, *J. Biol. Chem.* **2016**, *291*, 17816 – 17828.
[35] A. Hernández-Ortega, M. G. Quesne, S. Bui, D. J. Heyes, R. A. Steiner, N. S. Scrutton, S. P. de Visser, *J. Am. Chem. Soc.* **2015**, *137*, 7474 – 7487.
[36] P. F. Widboom, E. N. Fielding, Y. Liu, S. D. Bruner, *Nature* **2007**, *447*, 342 – 345.
[37] S. Fetzner, *Nat. Chem. Biol.* **2007**, *3*, 374 – 375.
[38] K. Li, E. N. Fielding, H. L. Condurso, S. D. Bruner, *Acta Crystallogr. Sect. D* **2017**, *73*, 573 – 580.
[39] C. T. Lohans, D. Y. Wang, J. Wang, R. B. Hamed, C. J. Schofield, *ACS Catal.* **2017**, *7*, 6587 – 6599.
[40] E. N. Fielding, P. F. Widboom, S. D. Bruner, *Biochemistry* **2007**, *46*, 13994 – 14000.
[41] P. F. Widboom, S. D. Bruner, *ChemBioChem* **2009**, *10*, 1757 – 1764.
[42] C. C. Tseng, F. H. Vaillancourt, S. D. Bruner, C. T. Walsh, *Chem. Biol.* **2004**, *11*, 1195 – 1203.
[43] N. V. Di Russo, H. L. Condurso, K. Li, S. D. Bruner, A. E. Roitberg, *Chem. Sci.* **2015**, *6*, 6341 – 6348.
[44] D. S. Kaliakin, D. G. Fedorov, Y. Alexeev, S. A. Varganov, *J. Chem. Theory Comput.* **2019**, *15*, 6074 – 6084.
[45] A. O. Lykhin, D. S. Kaliakin, G. E. dePolo, A. A. Kuzubov, S. A. Varganov, *Int. J. Quantum Chem.* **2016**, *116*, 750 – 761.
[46] A. O. Lykhin, S. A. Varganov, *Phys. Chem. Chem. Phys.* **2020**, *22*, 5500 – 5508.
[47] J. N. Harvey, *WIREs Comput. Mol. Sci.* **2014**, *4*, 1 – 14.
[48] J. N. Harvey, *Faraday Discuss.* **2004**, *127*, 165 – 177.
[49] J. N. Harvey, *Phys. Chem. Chem. Phys.* **2007**, *9*, 331 – 343.
[50] C. Zener, R. H. Fowler, *Proc. R. Soc. London Ser. A* **1932**, *137*, 696 – 702.
[51] G. E. dePolo, D. S. Kaliakin, S. A. Varganov, *J. Phys. Chem. A* **2016**, *120*, 8691 – 8698.
[52] P. J. Silva, M. J. Ramos, *J. Phys. Chem. B* **2007**, *111*, 12883 – 12887.
[53] P. J. Silva, M. J. Ramos, *Bioorg. Med. Chem.* **2008**, *16*, 2726 – 2733.
[54] S. Gómez-Carrasco, L. Gonzalez-Sanchez, A. Aguado, O. Roncero, J. M. Alvarado, M. L. Hernández, M. Paniagua, *J. Chem. Phys.* **2004**, *121*, 4605 – 4618.
[55] C. Sanz-Sanz, O. Roncero, M. Paniagua, A. Aguado, *J. Chem. Phys.* **2013**, *139*, 184302.
[56] A. Zanchet, F. Lique, O. Roncero, J. R. Goicoechea, N. Bulut, *Astron. Astrophys.* **2019**, *626*, A103.
[57] A. Zanchet, M. Menendez, P. G. Jambrina, F. J. Aoiz, *J. Chem. Phys.* **2019**, *151*, 094307.
[58] C. Sanz-Sanz, G. A. Worth, *Phys. Chem. Chem. Phys.* **2019**, *21*, 14429 – 14439.
[59] C. Sanz-Sanz, A. Aguado, O. Roncero, F. Naumkin, *J. Chem. Phys.* **2015**, *143*, 234303.
[60] G. Herzberg, *Spectra of Diatomic Molecules*, Van Nostrand Reinhold, New York, **1950**.
[61] M. A. El-Sayed, *J. Chem. Phys.* **1963**, *38*, 2834.
[62] H. Li, A. Kamasah, S. Matsika, A. G. Suits, *Nat. Chem.* **2019**, *11*, 123 – 128.
[63] C. Schweitzer, R. Schmidt, *Chem. Rev.* **2003**, *103*, 1685 – 1757.
[64] G. F. Minaev, *Int. J. Quantum Chem.* **1980**, *13*, 367 – 374.
[65] K. M. Ervin, I. Anusiewicz, P. Skurski, J. Simons, W. C. Lineberger, *J. Phys. Chem. A* **2003**, *107*, 8521 – 8529.
[66] S. Sharma, A. A. Holmes, G. Jeanmairet, A. Alavi, C. J. Umrigar, *J. Chem. Theory Comput.* **2017**, *13*, 1595 – 1604.
[67] A. A. Holmes, N. M. Tubman, C. J. Umrigar, *J. Chem. Theory Comput.* **2016**, *12*, 3674 – 3680.
[68] J. E. T. Smith, B. Mussard, A. A. Holmes, S. Sharma, *J. Chem. Theory Comput.* **2017**, *13*, 5468 – 5478.
[69] S. Jo, T. Kim, V. G. Iyer, W. Im, *J. Comput. Chem.* **2008**, *29*, 1859 – 1865.
[70] J. Lee, X. Cheng, J. M. Swails, M. S. Yeom, P. K. Eastman, J. A. Lemkul, S. Wei, J. Buckner, J. C. Jeong, Y. Qi, S. Jo, V. S. Pande, D. A. Case, C. L. Brooks, A. D. MacKerell, J. B. Klauda, W. Im, *J. Chem. Theory Comput.* **2016**, *12*, 405 – 413.
[71] B. R. Brooks, C. L. Brooks III, A. D. Mackerell, Jr., L. Nilsson, R. J. Petrella, B. Roux, Y. Won, G. Archontis, C. Bartels, S. Boresch, A. Caflisch, L. Caves, Q. Cui, A. R. Dinner, M. Feig, S. Fischer, J. Gao, M. Hodoscek, W. Im, K. Kuczera, T. Lazaridis, J. Ma, V. Ovchinnikov, E. Paci, R. W. Pastor, C. B. Post, J. Z. Pu, M. Schaefer, B. Tidor, R. M. Venable, H. L. Woodcock, X. Wu, W. Yang, D. M. York, M. Karplus, *J. Comput. Chem.* **2009**, *30*, 1545 – 1614.
[72] J. C. Phillips, R. Braun, W. Wang, J. Gumbart, E. Tajkhorshid, E. Villa, C. Chipot, R. D. Skeel, L. Kal'e, K. Schulten, *J. Comput. Chem.* **2005**, *26*, 1781 – 1802.
[73] J. Huang, S. Rauscher, G. Nawrocki, T. Ran, M. Feig, B. L. de Groot, H. Grubmuller, A. D. MacKerell, *Nat. Methods* **2017**, *14*, 71 – 73.
[74] A. D. MacKerell, M. Feig, C. L. Brook, *J. Am. Chem. Soc.* **2004**, *126*, 698 – 699.
[75] T. Darden, D. York, L. Pedersen, *J. Chem. Phys.* **1993**, *98*, 10089 – 10092.
[76] J.-P. Ryckaert, G. Ciccotti, H. J. C. Berendsen, *J. Comput. Phys.* **1977**, *23*, 327 – 341.
[77] V. Sharma, P. G. Jambrina, M. Kaukonen, E. Rosta, P. R. Rich, *Proc. Natl. Acad. Sci. USA* **2017**, *114*, E10339.
[78] H. L. Woodcock III, M. Hodoscek, A. T. B. Gilbert, P. M. W. Gill, H. F. Schaefer III, B. R. Brooks, *J. Comput. Chem.* **2007**, *28*, 1485 – 1502.
[79] Y. Shao, Z. Gan, E. Epifanovsky, A. T. B. Gilbert, M. Wormit, J. Kussmann, A. W. Lange, A. Behn, J. Deng, X. Feng, D. Ghosh, M. Goldey, P. R. Horn, L. D. Jacobson, I. Kaliman, R. Z. Khaliullin, T. Kús, A. Landau, J. Liu, E. I. Proynov, Y. M. Rhee, R. M. Richard, M. A. Rohrdanz, R. P. Steele, E. J. Sundstrom, H. L. Woodcock III, P. M. Zimmerman, D. Zuev, B. Albrecht, E. Alguire, B. Austin, G. J. O. Beran, Y. A. Bernard, E. Berquist, K. Brandhorst, K. B. Bravaya, S. T. Brown, D. Casanova, C.-M. Chang, Y. Chen, S. H. Chien, K. D. Closser, D. L. Crittenden, M. Diedenhofen, R. A. DiStasio Jr., H. Dop, A. D. Dutoi, R. G. Edgar, S. Fatehi, L. Fusti-Molnar, A. Ghysels, A. Golubeva-Zadorozhnaya, J. Gomes, M. W. D. Hanson-Heine, P. H. P. Harbach, A. W. Hauser, E. G. Hohenstein, Z. C. Holden, T.-C. Jagau, H. Ji, B. Kaduk, K. Khistyaev, J. Kim, J. Kim, R. A. King, P. Klunzinger, D. Kosenkov, T. Kowalczyk, C. M. Krauter, K. U. Lao, A. Laurent, K. V. Lawler, S. V. Levchenko, C. Y. Lin, F. Liu, E. Livshits, R. C. Lochan, A. Luenser, P. Manohar,

S. F. Manzer, S.-P. Mao, N. Mardirossian, A. V. Marenich, S. A. Maurer, N. J. Mayhall, C. M. Oana, R. Olivares-Amaya, D. P. O'Neill, J. A. Parkhill, T. M. Perrine, R. Peverati, P. A. Pieniazek, A. Prociuk, D. R. Rehn, E. Rosta, N. J. Russ, N. Sergueev, S. M. Sharada, S. Sharmaa, D. W. Small, A. Sodt, T. Stein, D. Stück, Y.-C. Su, A. J. W. Thom, T. Tsuchimochi, L. Vogt, O. Vydrov, T. Wang, M. A. Watson, J. Wenzel, A. White, C. F. Williams, V. Vanovschi, S. Yeganeh, S. R. Yost, Z.-Q. You, I. Y. Zhang, X. Zhang, Y. Zhou, B. R. Brooks, G. K. L. Chan, D. M. Chipman, C. J. Cramer, W. A. Goddard III, M. S. Gordon, W. J. Hehre, A. Klamt, H. F. Schaefer III, M. W. Schmidt, C. D. Sherrill, D. G. Truhlar, A. Warshel, X. Xua, A. Aspuru-Guzik, R. Baer, A. T. Bell, N. A. Besley, J.-D. Chai, A. Dreuw, B. D. Dunietz, T. R. Furlani, S. R. Gwaltney, C.-P. Hsu, Y. Jung, J. Kong, D. S. Lambrecht, W. Liang, C. Ochsenfeld, V. A. Rassolov, L. V. Slipchenko, J. E. Subotnik, T. Van Voorhis, J. M. Herbert, A. I. Krylov, P. M. W. Gill, M. Head-Gordon, *Mol. Phys.* **2015**, *113*, 184 – 215.

[80] S. Grimme, J. Antony, S. Ehrlich, H. Krieg, *J. Chem. Phys.* **2010**, *132*, 154104.

[81] S. Grimme, S. Ehrlich, L. Goerigk, *J. Comput. Chem*. **2011**, *32*, 1456 – 1465.

[82] H.-J. Werner, P. J. Knowles, G. Knizia, F. R. Manby, M. Schu"tz, P. Celani, W. Gy"orffy, D. Kats, T. Korona, R. Lindh, A. Mitrushenkov, G. Rauhut, K. R. Shamasundar, T. B. Adler, R. D. Amos, A. Bernhardsson, A. Berning, D. L. Cooper, M. J. O. Deegan, A. J. Dobbyn, F. Eckert, E. Goll, C. Hampel, A. Hesselmann, G. Hetzer, T. Hrenar, G. Jansen, C. K"oppl, Y. Liu, A. W. Lloyd, R. A. Mata, A. J. May, S. J. McNicholas, W. Meyer, M. E. Mura, A. Nicklass, D. P. O'Neill, P. Palmieri, D. Peng, K. Pflu"ger, R. Pitzer, M. Reiher, T. Shiozaki, H. Stoll, A. J. Stone, R. Tarroni, T. Thorsteinsson, M. Wang, M. Wellborn, *Molpro, version 2015.1, a package of ab initio programs*, **2015**, http://www.molpro.net.

[83] A. Zanchet, A. Dorta-Urra, A. Aguado, O. Roncero, *J. Phys. Chem. C* **2011**, *115*, 47 – 57.

[84] A. Zanchet, P. Lopez-Caballero, A. O. Mitrushchenkov, D. Buceta, M. A. Lopez-Quintela, A. W. Hauser, M. Pilar de Lara-Castells, *J. Phys. Chem. C* **2019**, *123*, 27064 – 27072.

[85] H.-J. Werner, P. J. Knowles, *J. Chem. Phys.* **1988**, *89*, 5803 – 5814.

[86] P. J. Knowles, H.-J. Werner, *Chem. Phys. Lett.* **1988**, *145*, 514 – 522.

[87] H.-J. Werner, P. J. Knowles, *J. Chem. Phys.* **1985**, *82*, 5053.

[88] P. J. Knowles, H.-J. Werner, *Chem. Phys. Lett.* **1985**, *115*, 259 – 267.

[89] A. Zanchet, L. Banares, M. L. Senent, A. Garcia Vela, *Phys. Chem. Chem. Phys.* **2016**, *18*, 33195 – 33203.

[90] G. Balerdi, J. Woodhouse, A. Zanchet, R. de Nalda, M. L. Senent, A. Garcia-Vela, L. Banares, *Phys. Chem. Chem. Phys.* **2016**, *18*, 110 – 118.

[91] S. Marggi Poullain, D. V. Chicharro, A. Zanchet, M. G. Gonzalez, L. Rubio-Lago, L. Banares, *Phys. Chem. Chem. Phys.* **2016**, *18*, 17054 – 17061.

[92] D. V. Chicharro, S. Marggi Poullain, A. Zanchet, A. Bouallagui, A. Garcia-Vela, M. L. Senent, L. Rubio-Lago, L. Bañares, *Chem. Sci.* **2019**, *10*, 6494 – 6502.

[93] Q. Sun, T. C. Berkelbach, N. S. Blunt, G. H. Booth, S. Guo, Z. Li, J. Liu, J. D. McClain, E. R. Sayfutyarova, S. Sharma, S. Wouters, G. Kin-Lic Chan, *Wiley Interdiscip. Rev.: Comput. Mol. Sci.* **2017**, *8*, e1340.

[94] J. Li, M. Otten, A. A. Holmes, S. Sharma, C. J. Umrigar, *J. Chem. Phys.* **2018**, *149*, 214110.

Manuscript received: June 22, 2020
Accepted manuscript online: September 25, 2020
Version of record online: December 14, 2020